RESEARCH ARTICLE

Powder Loading Effects on the Physicochemical and Mechanical Properties of 3D Printed Poly Lactic Acid/Hydroxyapatite Biocomposites

Cyron L. Custodio[1,2], Phoebeliza Jane M. Broñola[1], Sharyjel R. Cayabyab[1], Vivian U. Lagura[1], Josefina R. Celorico[1], and Blessie A. Basilia[1,2]*

[1]Materials Science Division, Industrial Technology Development Institute, Department of Science and Technology, Bicutan, Taguig City 1631, Philippines
[2]School of Graduate Studies, Mapúa University, Manila 1002, Philippines

Abstract: This study presents the physicochemical and mechanical behavior of incorporating hydroxyapatite (HAp) with polylactic acid (PLA) matrix in 3D printed PLA/HAp composite materials. Effects of powder loading to the composition, crystallinity, morphology, and mechanical properties were observed. HAp was synthesized from locally sourced nanoprecipitated calcium carbonate and served as the filler for the PLA matrix. The 0, 5, 10, and 15 wt. % HAp biocomposite filaments were formed using a twin-screw extruder. The resulting filaments were 3D printed in an Ultimaker S5 machine utilizing a fused deposition modeling technology. Successful incorporation of HAp and PLA was observed using infrared spectroscopy and X-ray diffraction (XRD). The mechanical properties of pure PLA had improved on the incorporation of 15% HAp; from 32.7 to 47.3 MPa in terms of tensile strength; and 2.3 to 3.5 GPa for stiffness. Moreover, the preliminary *in vitro* bioactivity test of the 3D printed PLA/HAp biocomposite samples in simulated body fluid (SBF) indicated varying weight gains and the presence of apatite species' XRD peaks. The HAp particles embedded in the PLA matrix acted as nucleation sites for the deposition of salts and apatite species from the SBF solution.

Keywords: Hydroxyapatite; Polylactic acid; 3D printing; Simulated body fluid

***Correspondence to:** Blessie A. Basilia, Materials Science Division, Industrial Technology Development Institute, Department of Science and Technology, Bicutan, Taguig City 1631, Philippines; basiliablessie@gmail.com

Received: November 6, 2020; **Accepted:** January 15, 2021; **Published Online:** January 28, 2021

Citation: Custodio CL, Broñola PJM, Cayabyab SR, *et al.,* 2021, Powder Loading Effects on the Physicochemical and Mechanical Properties of 3D Printed Poly Lactic Acid/Hydroxyapatite Biocomposites. *Int J Bioprint*, 7(1):326. http://doi.org/10.18063/ijb.v7i1.326

1. Introduction

Additive manufacturing, popularly known as three-dimensional (3D) printing, is a relatively useful and modern technology that promises excellent complex architectural control without requiring molds or templates, and the ability to tailor-fit designs depending on the demands specified by the end-user. The fabrication technology is mostly used for rapid prototyping to realize proof of concept ideas before large scale manufacturing. Another notable use of 3D printing is in the low-volume production of specific parts for specialized needs.

Industries where 3D printing has been involved include aerospace, automotive and transportation[1,2], military, medicine[3,4], construction[5,6], practical household items, and even clothing. All 3D printing technology print the object on some build platform that adjusts in height equal to the thickness of the layer being printed[7]. The coordinated printing motion relies on a 3D pattern created with a computer-aided design (CAD) software. A variety of printing techniques have been available for research, such as stereolithography (SLA)[8], selective laser sintering (SLS)[9], and fused deposition modeling (FDM)[10], to name a few. SLA utilizes ultraviolet (UV) light to polymerize and cure its liquid photoactive

monomer resin. The liquid resin solidifies on exposure to a CAD-guided incident light[8]. SLS traces a CAD pattern using a laser beam onto the powder resin, thus selectively sintering the powders into a solid object[9]. FDM extrudes a thermoplastic filament into built materials and support structures layer by layer[10]. Current commodity thermoplastic filaments that are suitable for FDM printing include polypropylene, acrylonitrile butadiene styrene, polystyrene, polyvinyl alcohol, polyamide (PA or nylon), and polylactic acid (PLA).

PLA has been a common filament for FDM 3D printing, mainly because of its relatively lower processing temperature, dimensional reliability, acceptable print quality, and good mechanical performance. Its monomer, lactic acid, is produced by fermenting dextrose derived from renewable crop resources such as corn, starch, and sugarcane. Hence, PLA is widely known as a sustainable, non-toxic biocompatible, and biodegrading material. To date, PLA is often used for biomedical applications, such as bone tissue engineering[11], scaffolds[12], and implants fabrication. PLA-based implants benefit from the avoidance of stress shielding effects, which is a known disadvantage for metal implants. While implanted inside the body, PLA would also dissolve naturally and is susceptible to biodegradation, and their by-products are non-toxic. Although plates and screws made from PLA have been used to fixate jaw fractures without additional support, PLA still has some inherent drawbacks and limitations. As compared to more popular bone implant materials such as stainless steel and alloy metals, PLA is comparatively inferior by a large margin in terms of mechanical performance. Another difficulty of using pure PLA is the poor cell attachment and proliferation on the polymer's surface. To address these concerns, the physicochemical properties of pure PLA can be altered and improved by incorporating biocompatible ceramic fillers and reinforcements.

Ceramic materials, such as calcium phosphates, silica, and alumina, comprise the human bone tissue. Due to their biocompatibility, these ceramic compounds have been synthesized and used as implants for biomedical applications. Bioactive implants are often coated with a type of calcium phosphate called hydroxyapatite (HAp, $Ca_{10}(PO_4)_6(OH)_2$), a promising bone substitute mineral. However, HAp is neither used for load-bearing applications nor in its bulk form due to its inherent brittleness. Therefore, HAp is mostly used as surface coating for other biomaterials dedicated for bone grafting. As a filler or reinforcing material, HAp can act to improve the matrix material's biocompatibility[13], stimulate bone regeneration, and improve the stiffness, compressive, and bending strengths[14]. Artificial implants should mimic the mechanical properties of the natural bone as close as possible. The human bone has stiffness in the range of 17–20 GPa. The integration of hard HAp ceramics and polymeric PLA matrix allows for bone substitute materials that are flexible and strong[14].

Injection-molded PLA/HAp bioactive composites have been fabricated to be used as an internal fixation device for cancellous bone regeneration[15]. Micro and nanoscale-HAp particles have been incorporated to PLA through electrospinning. Both micro-HAp and nano-HAp have shown to improve the elastic modulus of the electrospun mats and acted as nucleating agents. However, micro-HAp induced brittleness due to the bigger geometry of the fillers which acted as defects rather than as reinforcements[13]. A study on 3D printed PLA scaffolds varied the printing orientations (0°, 45°, and 90°), followed by surface modification using HAp. The resulting scaffolds' compressive properties and cell proliferation were observed. It was found that the optimal printing orientation was 90° as it produced the highest compressive strength (53 MPa), while no cell deaths were observed and all live cells have attached to the scaffold surface, thus ensuring the non-toxicity of the HAp-modified 3D printed PLA scaffolds[12].

In this study, Hap-reinforced PLA matrix biocomposites have been fabricated to determine the effects of HAp powder loading to the physicochemical and mechanical properties of the resulting 3D printed composite (**Figure 1**). From locally sourced nanoprecipitated calcium carbonate (NPCC), as-synthesized HAp powders were mechanically mixed with PLA at different powder loadings, followed by extrusion into a filament, and lastly 3D printed. The effect of the PLA/Hap composition on the crystallinity, morphology, and mechanical properties was investigated.

2. Materials and methods

2.1. Materials

NPCC was locally sourced from the Philippines. PLA pellets (PLA, NatureWorks LLC, IngeoTM Biopolymer 2003D) were purchased from D&L Polymers & Colors, Inc. The following chemicals: Phosphoric acid (H_3PO_4, RCI Labscan Ltd.), ammonium hydroxide (NH_4OH, Loba Chemie Pvt. Ltd.), and ethanol (CH_3CH_2OH, Thermo Fisher Scientific), were used without further purifications. Distilled water was used in preparing the solutions and for the washing procedures.

2.2. Hydroxyapatite synthesis

Chemical precipitation technique was undertaken using aqueous solution of calcium hydroxide, $Ca(OH)_2$ and H_3PO_4. Before synthesis, $Ca(OH)_2$ was prepared from the calcination of NPCC to decompose $CaCO_3$ into CaO and O_2 (Eq. 2.1). This was followed by slaking to convert CaO into

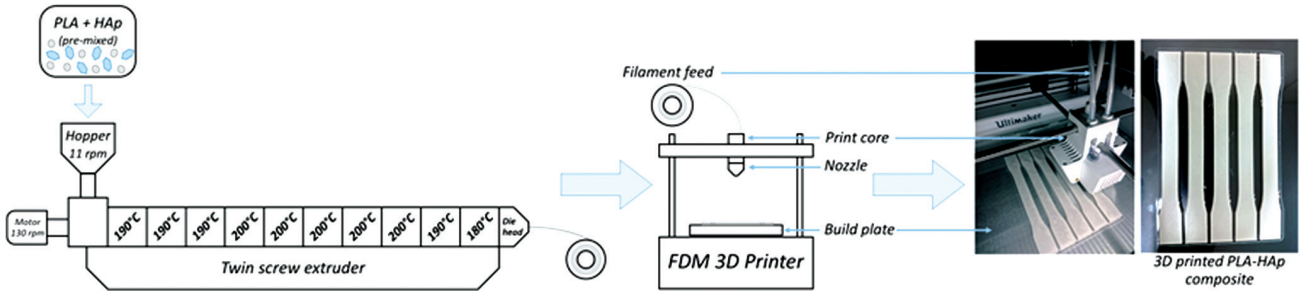

Figure 1. Schematic diagram of the polylactic acid/hydroxyapatite composite materials development process.

$Ca(OH)_2$ (Eq. 2.2). The obtained $Ca(OH)_2$ was dried and aqueous solution was prepared for the synthesis of HAp.

$$CaCO_3 \rightarrow CaO + CO_2 \quad (2.1)$$

$$CaO + H_2O \rightarrow Ca(OH)_2 \quad (2.2)$$

$$Ca(OH)_2 + H_3PO_4 \rightarrow Ca_{10}(PO_4)_6(OH)_2 \quad (2.3)$$

HAp was synthesized by mixing 1.5 M $Ca(OH)_2$ and 1 M H_3PO_4 (Eq. 2.3) at 40–50°C with continuous stirring. pH was monitored and maintained at 9–10 pH by dropwise addition of NH_4OH to the mixture. The reaction required a 48-h maturation period, followed by washing with ethanol, and finally neutralized using deionized water. Then, the as-synthesized HAp was dried, ball milled, and then passed through an 80-mesh sieve. Final drying step was done at 80°C. Finally, the dried HAp powders were calcined at 1100°C.

2.3. Extrusion of the PLA/HAp composite filament

HAp powders were mechanically mixed with PLA pellets at different powder loadings (0, 5, 10, and 15 wt%) before extrusion and were labeled as PLA/0H, PLA/5H, PLA/10H, and PLA/15H, respectively (**Table 1**). A twin-screw extruder (Labtech Engineering Co. Ltd., Thailand) with a nominal screw diameter of 20 mm was used to composite the PLA/HAp mixture. Based on the calorimetric data of the PLA precursor, the input temperature profile of the 10 extruder's heating zone blocks was 190°C, 190°C, 190°C, 200°C, 200°C, 200°C, 200°C, 200°C, 190°C, and 180°C, respectively (**Figure 1**). The PLA/HAp mixture was fed onto the hopper, with an 11 rpm feed rate, and the screw speed set to 130 rpm. On exiting the nozzle, the filament goes into a water bath for cooling down, followed by passing through an air blower, before finally consolidating in a rotating spooler. The desired filament diameter was achieved by manually controlling the extruder motor and spooling speeds. Before printing, the PLA/HAp composite filaments were stored in an airtight dry box at room temperature to reduce the ambient moisture absorption.

Table 1. Sample nomenclature and composition.

Sample	ID	% wt of HAp
PLA filled with 0% HAp	PLA/0H	0
PLA filled with 5% HAp	PLA/5H	5
PLA filled with 10% HAp	PLA/10H	10
PLA filled with 15% HAp	PLA/15H	15

PLA, polylactic acid; HAp, hydroxyapatite

2.4. 3D printing of the PLA/HAp composite filament

The composited PLA/HAp blends were loaded and fed onto a 3D printer (Ultimaker S5, Netherlands) which operates based on a FDM technology. The printing parameters are listed in **Table 2**. Basically, the filament feed is re-extruded through a ruby-tipped CC print core that is specifically designed for composites, which had a 0.6 mm nozzle. Print core temperature was set at 200°C (±10), while the build plate was set to 60°C. A CAD file guided the precise movement of the print core assembly, which includes the extrusion nozzle. To compensate for any non-uniformity of the filament diameter and potential under-extrusion, the material flow rate was adjusted from 100 to 200% to achieve an acceptable and uniform print quality.

Dumbbell-shaped tensile test specimens were then 3D printed. The specimen dimensions were adopted from ASTM D638, and the generated 3D model (.stl) was digitally drafted through a CAD software such as SolidWorks (Dassault Systemes, France). The (.stl) file of the design was sliced using the software Cura, an open source 3D printing slicing application, which converted the (.stl) file into the printable (.ufp) file format.

2.5. Digital microscopy

The digital microscope VHX-7000 (Keyence Corporation, Japan) was used to observe the surface

Table 2. 3D printing parameters for FDM printing of PLA/HAp composites.

Parameters	Settings
Layer height	0.2 mm
Infill density	100%
Infill pattern	Grid (45°, −45°)
Printing temperature	210°C
Build plate temperature	60°C
Print speed	45 mm/s
Extrusion width (nozzle diameter)	0.6 mm

PLA, polylactic acid; HAp, hydroxyapatite; FDM, fused deposition modeling.

features and textures, depth profile, and fractured cross section of the 3D printed PLA/HAp composites, as well as the resulting scaffolds immersed in simulated body fluid (SBF) solutions. The samples were observed from 30× to 500× range.

2.6. Chemical composition

Attenuated total reflectance-Fourier transform infrared (ATR-FTIR) spectra were recorded across the 4000–600 cm^{-1} frequency range, with 1–2 μ penetrating depth, and with 20 scans per sample at room temperature (23°C) using a Frontier FTIR spectrometer (PerkinElmer, USA). The synthesized HAp and 3D printed PLA/HAp composites were subjected to ATR-FTIR scans to determine the functional groups within the composite material.

2.7. Crystallinity

The diffraction patterns were obtained using a LabX X-ray diffraction (XRD)-6000 X-ray diffractometer (Shimadzu, Japan), with a Cu Kα radiation source at 40 kV operating voltage. The scanned range for all samples was from 2° to 60° (2θ) with a step size of 1°/min. The synthesized HAp, 3D printed PLA/HAp composites, and the biomineralized scaffolds were subjected to XRD characterization to confirm the presence of apatite species and their influence to the composite.

2.8. Mechanical properties

As adopted from ASTM D638, the tensile tests were carried out using a universal testing machine (Instron 5585H, USA), with a 10 kN static load cell, at a gauge length of 50 mm, and a strain rate of 5 mm/min. Tensile tests were done to determine the elastic modulus and tensile strength of the 3D printed PLA/HAp biocomposites. Five trials were tested for each sample, the average values reported, and the representative samples were plotted. Width and thickness of the test specimens were measured using a Mitutoyo digital caliper before testing. The tests were performed at room temperature and 54% relative humidity.

2.9. *In vitro* biomineralization

The bioactivities of the 3D printed scaffolds were assessed through immersion in SBF. The scaffolds were immersed in an SBF solution having a composition similar to what Rodriguez and Gatenholm reported[16], to determine the effect of increasing HAp powder loading to their biomineralization activity as a function of time. A liter of SBF solution was prepared by dissolving the analytic grade reagents (< 99%) in distilled water in the following order shown in **Table 3**.

In preparing the SBF solution, each reagent was added after the previous reagent has dissolved completely. The solution was prepared at 36.5°C under constant stirring. The pH of the solution was also adjusted to pH 7.4 using 1 M HCl solution and was kept refrigerated at 4°C before usage. The SBF is similar to the human blood plasma ionic concentration and composition. The samples were immersed in 15 mL of SBF solution and placed inside a dedicated oven set at 37°C for 24, 48, and 72 h to assess the growth and deposition of apatite species on the scaffold[17,18]. The SBF-immersed samples were retrieved from the solution and dried in the oven overnight, and finally characterized through digital microscopy, gravimetric analysis, and XRD.

3. Results and discussion

3.1. 3D printed PLA/HAp prototype

Figure 2 shows the digital micrographs of the 3D printed PLA/HAp composites at different magnification levels, including the depth profile analysis. The top view of pure PLA (PLA/0H) was characterized by well-defined individual print beads, as the grid could be clearly seen both from 30× to 200× (**Figure 2A and B**), and even at the depth profile (**Figure 2E-F**). However, as the HAp loading was increased from 5 wt% to 15 wt%, the print beads were slowly disappearing and became less defined. Likewise, the surface finish oh PLA/5H, PLA/10H, and PLA/15H were more irregular and rougher than PLA/0H. The same visual trend could be seen at the depth profile, whereas the print bead gaps were slowly closing in and disappearing (**Figure 2L, R and X**). Hence, the 3D printed PLA/HAp composites were becoming more irregular as the HAp loadings were increased. Nonetheless, hydroxyapatite powders were seen from the composite surface with increasing frequency in accordance to the increasing HAp loading, although the distribution were irregular and agglomeration was present (**Figure 2H, J, N, P, T and V**).

Porosity and density are also some physical properties that must be considered, especially with polymer matrix composites. These properties can provide useful information in the prediction of the material's behavior, for instance, under mechanical stimuli. A denser material is usually a stronger one, and a porous material is usually

Table 3. Reagents and composition of the simulated body fluid solution.

Chemical reagent		Formula weight (g/mol)	Weight (g or mL in 1 L solution)
Sodium chloride	NaCl, Univar	58.44	7.996 g
Sodium bicarbonate	$NaHCO_3$, Loba Chemie	84.01	0.350 g
Potassium chloride	KCl, TPC	74.55	0.224 g
Potassium phosphate dibasic anhydrous	K_2HPO_4, Loba Chemie	174.18	0.228 g
Magnesium chloride hexahydrate	MgCl·6H2O, Loba Chemie	203.3	0.305 g
Hydrochloric acid (1 M)	HCl, LabScan	36.458	40 mL
Calcium chloride dihydrate	$CaCl_2 \cdot 2H_2O$, TPC	147.02	0.278 g
Sodium sulfate anhydrous	Na_2SO_4, Fisher Scientific	142.02	0.071 g
Tris buffer	$NH_2C(CH_2OH)_3$ Loba Chemie	121.14	6.057 g

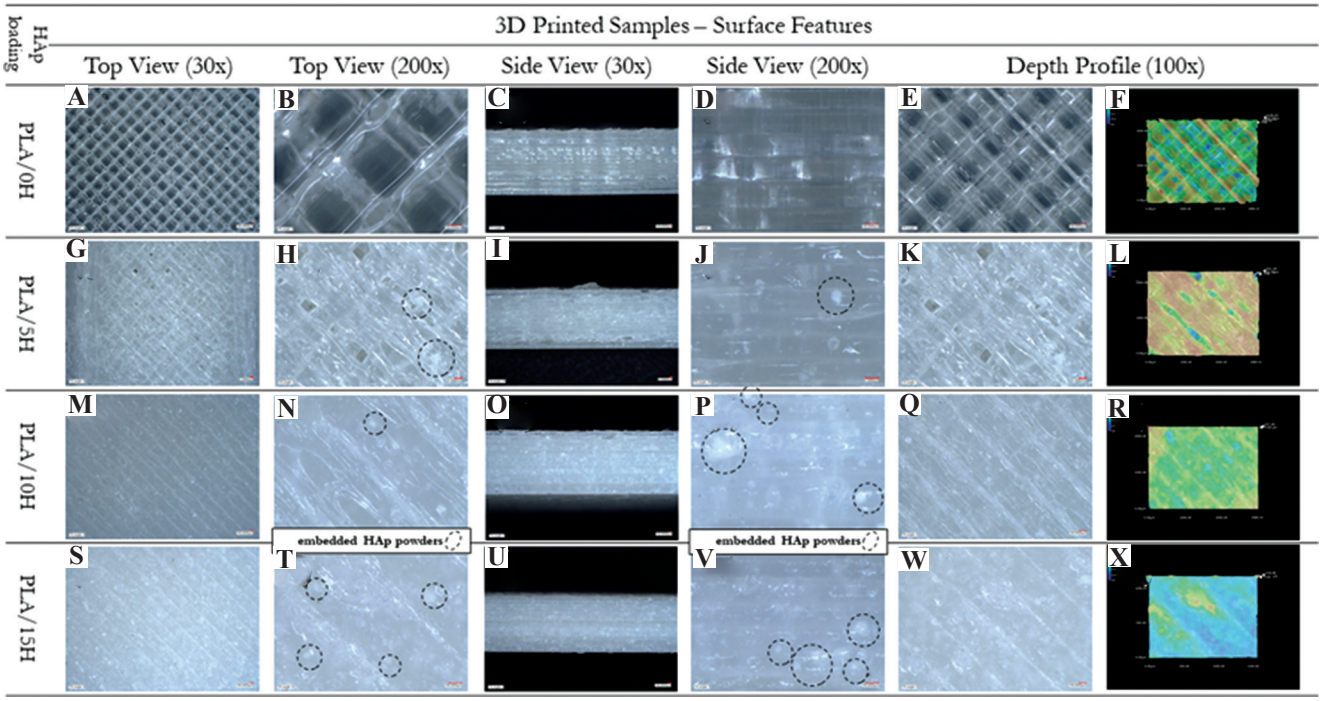

Figure 2. Digital micrographs of 3D printed polylactic acid (PLA)/hydroxyapatite: (A-F) PLA/0H; (G-L) PLA/5H; (M-R) PLA/10H; and (S-X) PLA/15H.

mechanically inferior. The experimental density and true porosity are presented in **Figures 3A and B**, respectively. We can see that as the HAp loading was increased, in an opposite manner the composites' density decreased. On the other hand, the porosity kept increasing, which means that more voids were forming as more HAp was added. Perhaps the tendency of HAp particles to agglomerate influenced the composites' microstructure and developed two kinds of sites that were agglomerated and areas that were porous as well. The true porosity was calculated using the following equation:

$$(\%)\mathrm{P} = 1 - \frac{\rho_{experimental}}{\rho_{theoretical}} \times 100 \qquad (3.1)$$

Where P refers to the true porosity (in percent), $\rho_{experimental}$ refers to experimental density, and $\rho_{theoretical}$ refers to theoretical density. The literature theoretical densities of ρ_{PLA} and ρ_{HAp} are 1.43 g•cm^{-3} and 3.16 g•cm^{-3}, respectively[19].

3.2. Chemical composition

The changes in absorbance or absence of certain peaks in the FTIR spectra are presented in **Figure 4**. These absorption peaks can be attributed to functional groups that are present in HAp, in pure PLA, or in the composite material. Peaks and functional groups originating from PLA were located approximately at 2996 cm^{-1} and 2945 cm^{-1} (CH_3 stretching). The peaks at 1748 cm^{-1},

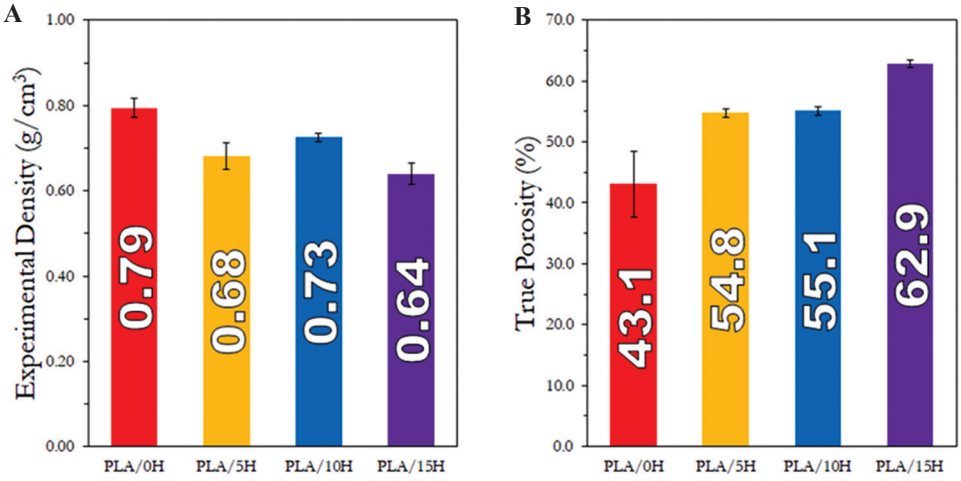

Figure 3. (A) Experimental density and (B) true porosity of the 3D printed polylactic acid /hydroxyapatite composites.

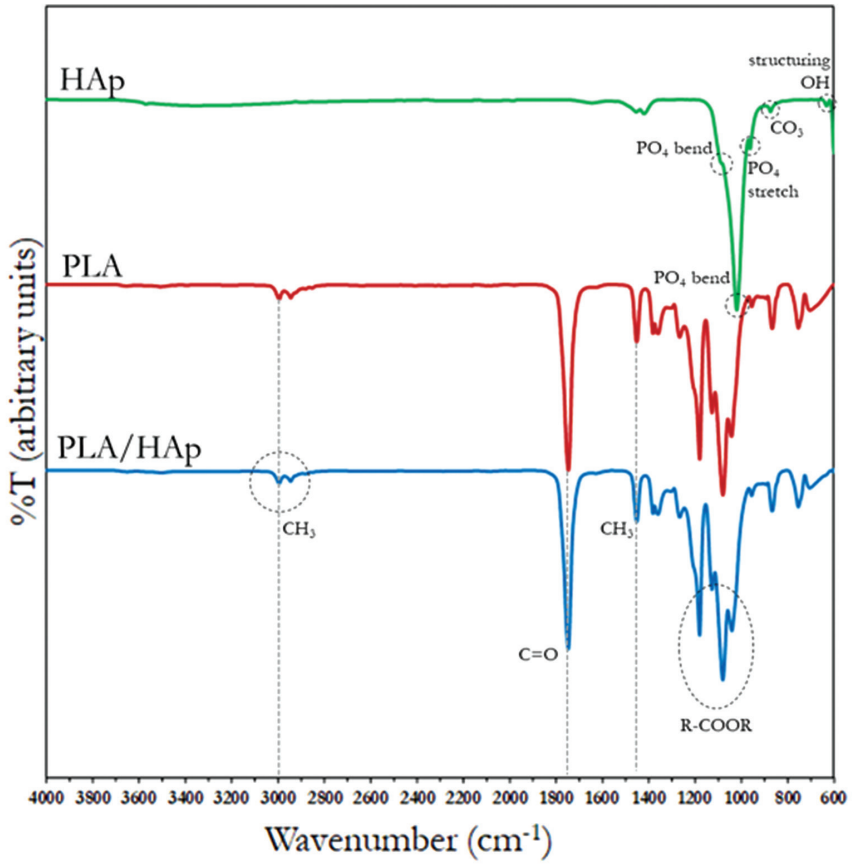

Figure 4. Fourier transform infrared spectra of hydroxyapatite (Hap), polylactic acid (PLA), and the 3D printed PLA/HAp composite (15 wt. %).

1181 cm^{-1}, 1127 cm^{-1}, and 1080 cm^{-1} are identified as the backbone of ester groups of PLA[20]. Furthermore, 1748 cm^{-1} pertains to C=O stretching vibrations[21], the peak at 1045 cm^{-1} for the OH bending, while the 1200–1000 cm^{-1} refers to C-O stretching[22].

Peaks coming from HAp are generally from phosphate groups, such as 1090 cm^{-1}, 1030 cm^{-1}, 600 cm^{-1}, and 565 cm^{-1} (PO_4 bending), and 960 cm^{-1} (PO_4 stretching). Carbonate ions were faintly present at 870 cm^{-1}[11,13]. The high calcining temperature of 1100°C in the HAp synthesis has caused the removal of water (as suggested by the absence of 3600–3200 cm^{-1} OH stretch). The visibility of the structuring OH was identified at 635 cm^{-1} fingerprint region, indicating a better powder-polymer

adhesion. However, the high calcination temperature might have also caused aggregation which prevented good dispersion of HAp powders in the PLA matrix[14]. The few prominent peaks of HAp were observed to be overlapped by the more intense peaks of PLA, approximately around 1100–900 cm^{-1}. Moreover, no new covalent bonds formed within the PLA/HAp composites, suggesting that the HAp fillers were embedded in the polymer matrix through mechanical manner rather than by chemical means.

3.3. Crystallinity

XRD of HAp, PLA, and the printed PLA/HAp biocomposites is shown in **Figure 5**. The HAp diffractogram displayed the crystalline nature of the powder. Prominent peaks and their corresponding planes were noted at approximately 26° (002), 33° (112), 47° (222), and 49° (213). The (211) plane at ca. 32° is inherent to and characteristic of pure HAp[12].

Pure PLA (PLA/0H) exhibited a broad spectrum indicating the amorphous structure of the polymer[23]. The composite samples exhibited diffraction peaks characterized by the presence of HAp in the polymer matrix. The peak intensity increases as a function of the increase in HAp powder loading.

3.4. Mechanical properties

The tensile stress-strain curve of PLA/HAp biocomposites is shown in **Figure 6A**. The HAp indeed had a reinforcing effect, as the elastic moduli and tensile strengths both increased compared to pure PLA. As the powder loading was increased, the elastic modulus increased compared to pure PLA (2.3–~3.5 GPa), but the modulus remained consistent despite the further increase in HAp loading (**Figure 6B**). Unsurprisingly, the tensile strength decreased at 15 wt% HAp loading as the powder loading increased. This may be primarily due to the HAp agglomeration and poor dispersion, as well as the formation of macro voids between neighboring filament beads. Nevertheless, HAp has shown to improve the strength of pure PLA (32.7–47.3 MPa). HAp might also act as nucleation sites where PLA molecule chains could have entangled itself through mechanical interlocking effects.

The stiffness of both PLA/10H and PLA/15H similarly generated 3.5 GPa elastic modulus which is within the range of the human cancellous bone tissue[15]; hence, these formulations have the potential for the repair of smaller bone tissues.

The fracture surface after the uniaxial tensile testing of PLA/HAp biocomposites are shown in

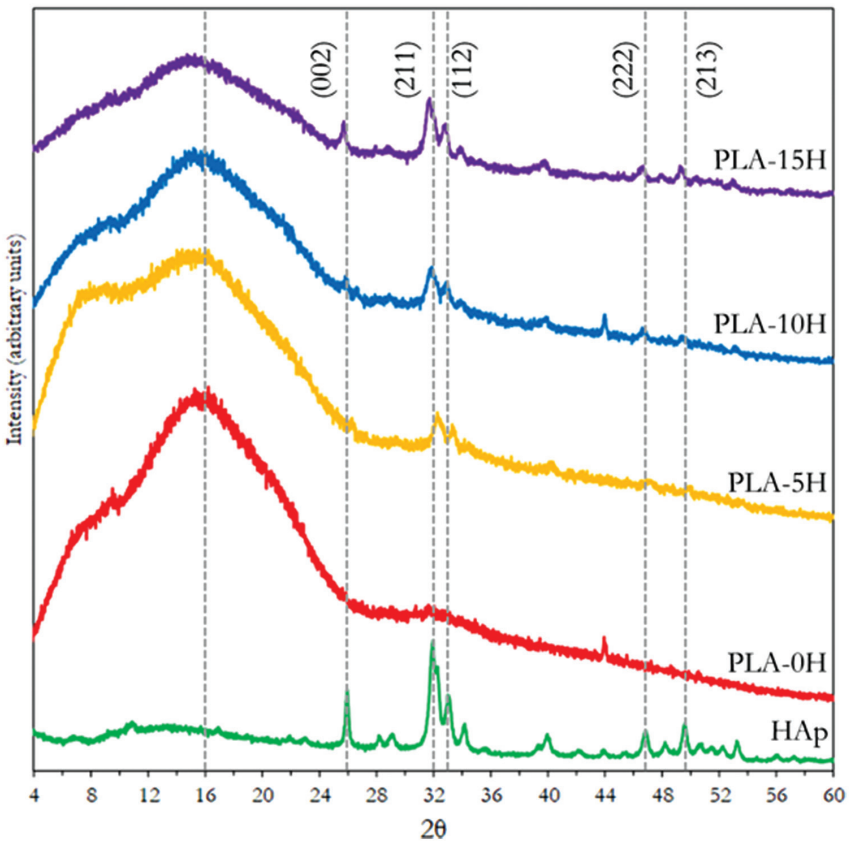

Figure 5. X-ray diffractograms of hydroxyapatite (HAp), and varying powder loading in 3D printed polylactic acid/HAp composites (0–15 wt. %).

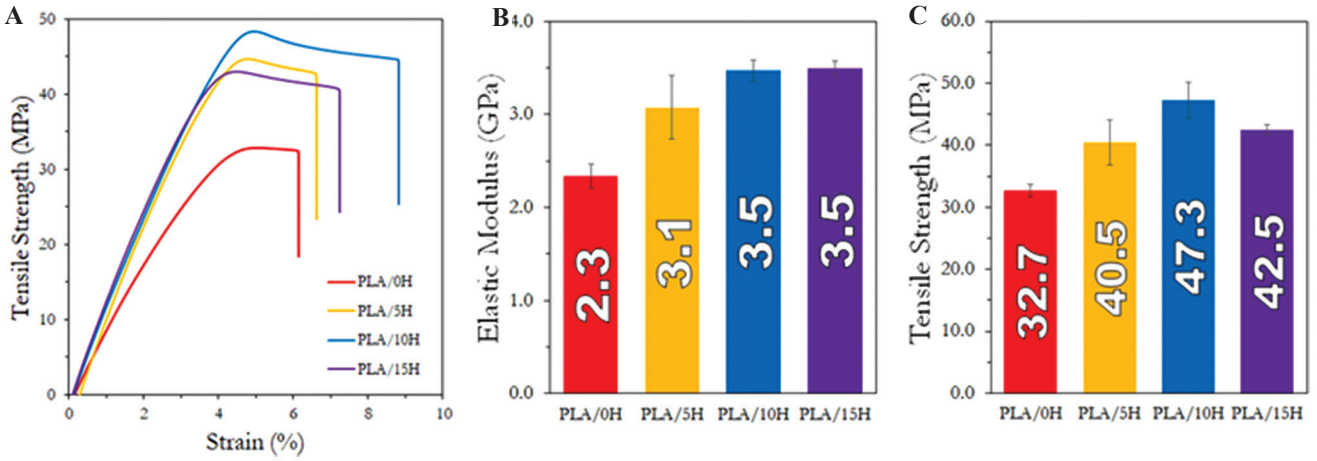

Figure 6. (A) Tensile stress-strain graph, (B) elastic moduli, and (C) tensile strength of the 3D printed polylactic acid/hydroxyapatite composites.

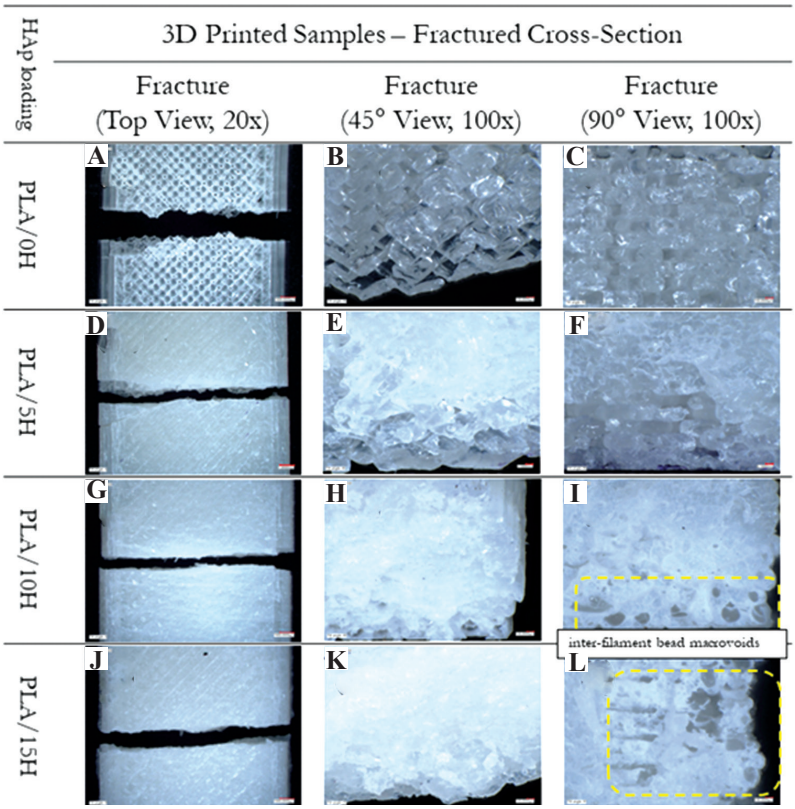

Figure 7. Fracture surfaces of the tensile-tested 3D printed polylactic acid (PLA)/hydroxyapatite composites. (A-C) PLA/0H; (D-F) PLA/5H; (G-I) PLA/10H; and (J-L) PLA/15H.

Figure 7. Fracture surfaces can provide knowledge and insight on the interaction between the matrix and reinforcement upon the application of force. The tensile-tested PLA/HAp composites exhibited linear, brittle fractures (**Figure 7D, G and J**), contrary to the somewhat irregular, moderately ductile fracture from the PLA/0H sample (**Figure 7A**). Furthermore, at higher magnifications (**Figure 7B, E and H, K**) the individual print beads were slowly disappearing as the HAp loading was increased. Evolution of macro voids or pores were also noticeable at higher magnifications (**Figure 7 I and L**). These macro voids account for the decreasing density and likewise increasing porosity from **Figure 3**. A plausible explanation can be attributed to the agglomeration of HAp particles,[15] which causes some areas to be denser and consequently

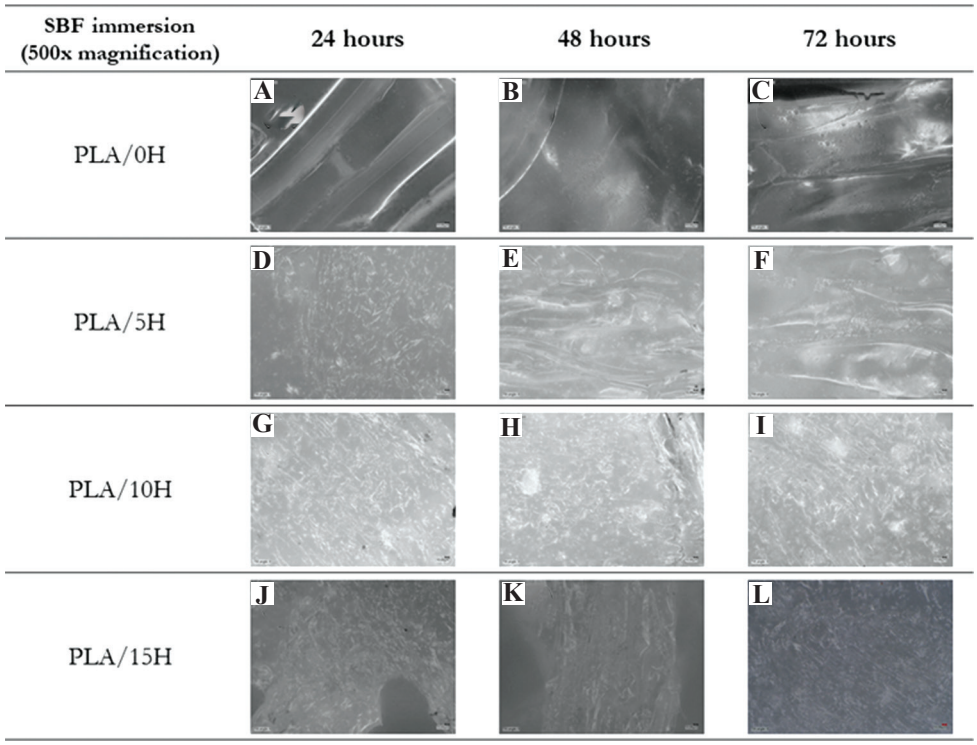

Figure 8. Digital micrographs of 3D printed polylactic acid/hydroxyapatite scaffolds immersed for 72 h in simulated body fluid for biomineralization activity.

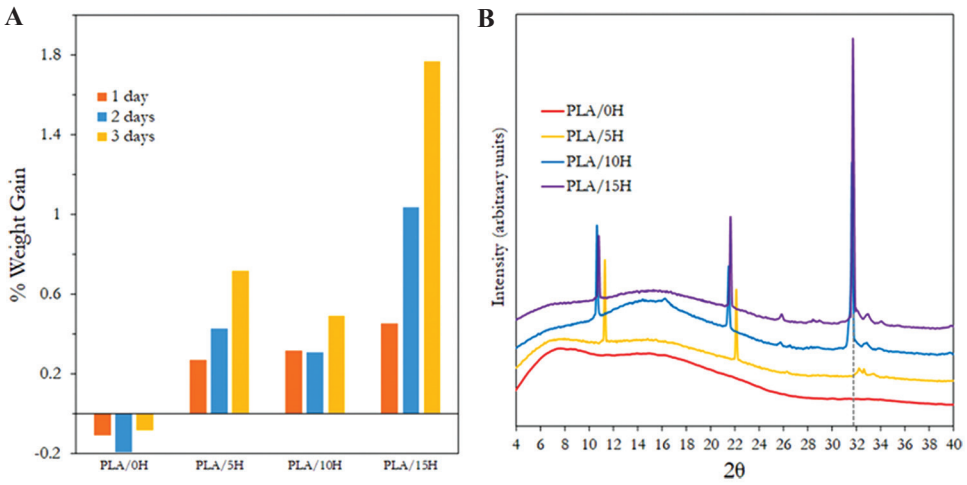

Figure 9. (A) Weight gain (%) and (B) X-ray diffractograms of the 3D printed polylactic acid/hydroxyapatite composites after the 72-h immersion test in SBF.

creating other sites with less material leading to void formation.

3.5. *In vitro* biomineralization

A preliminary *in vitro* bioactivity test was done by immersing the 3D printed PLA/HAp composite samples in SBF solutions for 24, 48, and 72 h, and the digital micrograph results are shown in **Figure 8**, while the percent weight gain and X-ray diffractograms are shown in **Figure 9A and B**, respectively. As seen on the digital micrographs, the 3D printed pure PLA (PLA/0H) exhibited an etching response to soaking in SBF. This was supported by the mass loss in **Figure 9A**. Pure PLA remains to be partly hydrophilic, and hence subjecting it to an aqueous immersion resulted to some PLA dissolving away.

The PLA/HAp composites reported varying weight gains, with the trend that was increasing. HAp particles

embedded within the PLA matrix served as nucleation sites for the deposition of calcium salts and apatite species present from the SBF solution. X-ray diffractograms shown in **Figure 9B** report of the evolution of peaks after the immersion in SBF for 72 h. The characteristic peak at 2θ ~32° confirm the growth of apatite species on the 3D printed samples during the immersion bioactivity[18]. Other well-defined peaks could be attributed to other salt species present in the SBF solution being deposited onto the 3D printed substrates.

4. Conclusion

The HAp used in this study was successfully synthesized as confirmed by the FTIR and XRD spectra. Pure PLA exhibited a broad infrared spectrum indicating the amorphous structure of the polymer. The 3D printed PLA/HAp composite samples exhibited XRD diffraction peaks characterized by the presence of HAp with the peak intensity increasing as a function of HAp powder loading. Moreover, composites' density decreases as the HAp loading was increased. The elastic modulus increased from 2.3 to 3.5 GPa and the tensile strength increased from 32.7 to 47.3 MPa with 15% HAp loading. The preliminary *in vitro* bioactivity test of the 3D printed PLA/HAp composite samples in SBF solutions for 24, 48, and 72 h indicated varying weight gains progressively as well as the evolution of XRD peaks. These indicate that HAp particles embedded within the PLA matrix served as nucleation sites for the deposition of calcium salts and apatite species present from the SBF solution.

Author contributions

B.A.B. led the project and edited the paper. J.R.C., C.L.C., and P.J.M.B. designed the study. P.J.M.B. and S.R.C. performed the HAp synthesis and biomineralization, respectively. P.J.M.B. and C.L.C. performed the filament extrusion. C.L.C. performed most experiments, 3D printing, characterizations, data analysis, and wrote the paper with help from V.U. L. and J.R.C.

Conflicts of interest

The authors declare that they have no conflicts of interest.

Acknowledgments

We acknowledge the funding of this research project from the Department of Science and Technology – Grants-In-Aid (Department of Science and Technology [DOST]-GIA). We are also grateful for the technical support provided by the Advanced Device and Materials Testing Laboratory, and the Standards and Testing Division of the Industrial Technology Development Institute of the DOST, Philippines.

References

1. Najmon JC, Raeisi S, Tovar A, 2019, Review of Additive Manufacturing Technologies and Applications in the Aerospace Industry. Additive Manufacturing for the Aerospace Industry. Elsevier Inc., Amsterdam, Netherlands. https://doi.org/10.1016/b978-0-12-814062-8.00002-9
2. Wiese M, Thiede S, Herrmann C, 2020, Rapid Manufacturing of Automotive Polymer Series Parts: A Systematic Review of Processes, Materials and Challenges. *Addit Manuf*, 36:101582. https://doi.org/10.1016/j.addma.2020.101582
3. Ng WL, Chua CK, Shen YF, 2019, Print Me An Organ! Why We Are Not There Yet. *Prog. Polym. Sci*., 97:101145. https://doi.org/10.1016/j.progpolymsci.2019.101145
4. Lee JM, Ng WL, Yeong WY, 2019, Resolution and Shape in Bioprinting: Strategizing Towards Complex Tissue and Organ Printing. *Appl. Phys. Rev*., 6:011307. https://doi.org/10.1063/1.5053909
5. Lao W, Li M, Wong TN, *et al*., 2020, Improving Surface Finish Quality in Extrusion-based 3D Concrete Printing Using Machine Learning-based Extrudate Geometry Control. *Virtual Phys Prototyp*, 15:178–93. https://doi.org/10.1080/17452759.2020.1713580
6. Ahmed ZY, Bos FP, van Brunschot MCA, *et al*., 2020, On-demand Additive Manufacturing of Functionally Graded Concrete. *Virtual Phys Prototyp*, 15:194–210. https://doi.org/10.1080/17452759.2019.1709009
7. Alizadeh-Osgouei M, Li Y, Wen C. 2019, A Comprehensive Review of Biodegradable Synthetic Polymer-ceramic Composites and their Manufacture for Biomedical Applications. *Bioact Mater*, 4:22–36. https://doi.org/10.1016/j.bioactmat.2018.11.003
8. Ng WL, Lee JM, Zhou M, *et al*., 2020, Vat Polymerization-based Bioprinting Process, Materials, Applications and Regulatory Challenges. *Biofabrication*, 12:022001. https://doi.org/10.1088/1758-5090/ab6034
9. Gayer C, Ritter J, Bullemer M, *et al*., 2019, Development of a solvent-free polylactide/calcium carbonate composite for selective laser sintering of bone tissue engineering scaffolds. *Mater Sci Eng C*, 101:660–73. https://doi.org/10.1016/j.msec.2019.03.101
10. Percoco G, Uva AE, Fiorentino M, *et al*., 2020, Mechanobiological Approach to Design and Optimize Bone Tissue Scaffolds 3D Printed with Fused Deposition Modeling: A Feasibility Study. *Materials* (*Basel*), 13: 648. https://doi.org/10.3390/ma13030648

11. Hassanajili S, Karami-Pour A, Oryan A, *et al*., 2019, Preparation and Characterization of PLA/PCL/HA Composite Scaffolds Using Indirect 3D Printing for Bone Tissue Engineering. *Mater Sci Eng C*, 104:109960. https://doi.org/10.1016/j.msec.2019.109960
12. Mondal S, Phuoc T, Pham VH, *et al*., 2019, Hydroxyapatite Nano Bioceramics Optimized 3D Printed Poly Lactic Acid Scaffold for Bone Tissue Engineering Application. *Ceram Int*, 46:1–13. https://doi.org/10.1016/j.ceramint.2019.10.057
13. Lopresti F, Pavia FC, Vitrano I, *et al*., 2020, Effect of Hydroxyapatite Concentration and Size on Morpho-mechanical Properties of PLA-based Randomly Oriented and Aligned Electrospun Nanofibrous Mats. *J Mech Behav Biomed Mater*, 101:103449. https://doi.org/10.1016/j.jmbbm.2019.103449
14. Pietrzykowska E, Mukhovskyi R, Chodara A, *et al*., 2019, Composites of Polylactide and Nano-Hydroxyapatite Created by Cryomilling and Warm Isostatic Pressing for Bone Implants Applications. *Mater Lett*, 236:625–8. https://doi.org/10.1016/j.matlet.2018.11.018
15. Prasad A, Bhasney S, Katiyar V, *et al*., 2017, Biowastes Processed Hydroxyapatite filled Poly (Lactic acid) Bio-Composite for Open Reduction Internal Fixation of Small Bones. *Mater Today Proc*, 4:10153–7. https://doi.org/10.1016/j.matpr.2017.06.339
16. Rodríguez K, Renneckar S, Gatenholm P, 2011, Biomimetic Calcium Phosphate Crystal Mineralization on Electrospun Cellulose-based Scaffolds. *ACS Appl Mater Interfac*, 3:681–9. https://doi.org/10.1021/am100972r
17. Hamzah MSA, Ng C, Zulkarnain NI, *et al*., 2020, Entrapment of Collagen on Polylactic Acid 3D Scaffold Surface as a Potential Artificial Bone Replacement. *Mater Today Proc*, 2020:263. https://doi.org/10.1016/j.matpr.2020.07.263
18. Alam F, Varadarajan KM, Kumar S, 2020, 3D Printed Polylactic Acid Nanocomposite Scaffolds for Tissue Engineering Applications. *Polym Test*, 81:106203. https://doi.org/10.1016/j.polymertesting.2019.106203
19. Nawawi AN, Alqap SF, Sopyan I, 2011, Recent Progress on Hydroxyapatite-based Dense Biomaterials for Load Bearing Bone Substitutes. *Recent Patents Mater Sci*, 4:63–80. https://doi.org/10.2174/1874464811104010063
20. Lizundia E, Vilas JL, León LM, 2015, Crystallization, Structural Relaxation and Thermal Degradation in Poly(l-lactide)/Cellulose Nanocrystal Renewable Nanocomposites. *Carbohydr Polym*, 123:256–65. https://doi.org/10.1016/j.carbpol.2015.01.054
21. Xu C, Chen J, Wu D, *et al*., 2016, Polylactide/Acetylated Nanocrystalline Cellulose Composites Prepared by a Continuous Route: A Phase Interface-property Relation Study. *Carbohydr Polym*, 146:58–66. https://doi.org/10.1016/j.carbpol.2016.03.058
22. Gazzotti S, Farina H, Lesma G, *et al*., 2017, Polylactide/Cellulose Nanocrystals: The *in situ* Polymerization Approach to Improved Nanocomposites. *Eur Polym J*, 94:173–84. https://doi.org/10.1016/j.eurpolymj.2017.07.014
23. Bhasney SM, Bhagabati P, Kumar A, *et al*., 2019, Morphology and Crystalline Characteristics of Polylactic Acid [PLA]/Linear Low Density Polyethylene [LLDPE]/Microcrystalline Cellulose [MCC] Fiber Composite. *Compos Sci Technol*, 171:54–61. https://doi.org/10.1016/j.compscitech.2018.11.028